Islamic Azad University

Journal of

Optoelectronical Nanostructures

Winter 2016 / Vol. 1, No. 4

Quantum modeling of light absorption in graphene based photo-transistors

Hamid Faezinia[1], **Mahdi Zavvari**[*,2]

[1] Department of Electronic Engineering, Tabriz Branch, Islamic Azad University, Tabriz, Iran.

[2] Department of Electronic Engineering, Urmia Branch, Islamic Azad University, Urmia, Iran.

(Received 22 Dec. 2016; Revised 19 Jan. 2017; Accepted 23 Feb. 2017; Published 15 Mar. 2017)

Abstract: Graphene based optical devices are highly recommended and interested for integrated optical circuits. As a main component of an optical link, a photodetector based on graphene nano-ribbons is proposed and studied. A quantum transport model is presented for simulation of a graphene nano-ribbon (GNR) -based photo-transistor based on non-equilibrium Green's function method. In the proposed model a self-energy matrix is introduced which takes the effect of optical absorption in GNR channel into account. The self-energy matrix is treated as a scattering matrix which leads to creation of carriers. The transition matrix element is calculated for optical absorption in graphene channel and is used to obtain the optical interaction self-energy. The resulting self-energy matrix is added to retarded Green's function and is used in transport equations for calculation of current flow in the photo-transistor. By considering the effect of optical radiation, the dark and photocurrent of detector are calculated and results are used for calculation of responsivity.

Keywords: Non-equilibrium Green's function; Graphene nano-ribbon; Photo-transistor; Self-energy.

1. Introduction

Recently graphene based electronic and optoelectronic devices have been attracted much interest because of excellent properties of graphene layers [1-5]. Interestingly, graphene could be patterned in nano-ribbons, by some fabrication

[*] **Corresponding author. E-mail: m.zavvari@iaurmia.ac.ir**

technologies as electron beam lithography and etching, [6-8] to have properties from metallic to semiconducting depending on their width and edges [9, 10]. This band-gap tuning capability and the possibility of large-scale integration using planar technologies open a route towards an all-graphene electronic nano-devices and circuits [11, 12]. On the other hand, graphene exhibits unique optical and electronic properties making it suitable for optoelectronic applications [13, 14]. As one of these optical applications, graphene photodetector can operate over a broad wavelength range from the ultraviolet to terahertz while photodetectors of IV and III-V semiconductor suffer from long-wavelength limit due to large bandgap [15, 16]. Some groups have reported experimental developments of graphene photodetectors however theoretical modeling of these detectors is still limited [17-20]. Gao et al. developed a quantum mechanical approach to predict the optical performance of graphene photodetectors, however in their model the effect of optical input intensity is missed and hence it is difficult to obtain some important properties of a detector such as responsivity and detectivity [21]. On the other hand, Ahmadi et al. presented a modeling approach for graphene based photodetectors but their model is too genera and does't consider the band-structure and energy diagram of graphene layers [22].

In this paper, we use a quantum transport approach and extend it to include the effect of optical input power and investigate the properties of graphene based photo-transistors. In this model, we use the concept of self-energy to account for the contacts (like the source and drain) to the channel. To include the effect of photon absorption, an additional optical self-energy matrix is also introduced in Green's function based transport equations. By calculation of photo-current flow in detector and under light illumination the performance of the detector could be studied for different input powers. The paper is organized as following. In the section 2 the modeling procedure and calculation methods are described and results and discussions are in section3. The paper is concluded in section 4.

2. SIMULATION APPROACH

The schematic of proposed GNR based photo-transistor is shown in Fig. 1. As can be seen in figure, there is a conducting GNR channel between source and drain contacts whose current is controlled by the voltages dropped in gate contact. In order to model the behavior of this device, a non-equilibrium Green's function

(NEGF) method is used. The basis of this method is obtaining the retarded Green's function related to the structure using the following equation [23]:

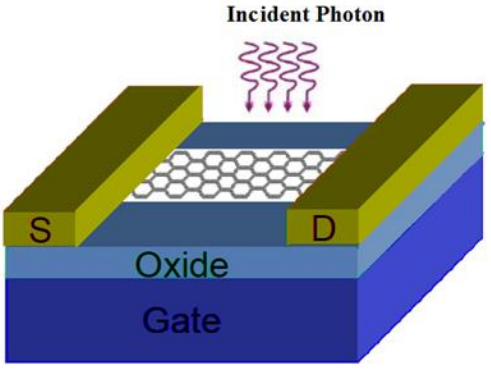

Fig. 1. Schematic of GNR photo-transistor.

$$G(E)=\left[EI-H-\sum_S-\sum_D\right]^{-1} \quad (1)$$

where Σ_S, Σ_D, H , E, and I are self-energy of the source contact, self-energy of the drain contact, Hamiltonian matrix, energy, and unit matrix, respectively.
The approach of the none equilibrium Green's function is to find the appropriate Green's function according to eq.(1) in which the inverse matrix should be calculated for every energy level. Using conventional methods, a bigger matrix should be inverted, which is time consuming and impractical for the simulation of structures in such dimensions. However, in ballistic conditions, the solution will be simple, due to the fact that fewer columns of the matrix related to the Green's function are needed. The Hamiltonian matrix can be realized in two ways [24]: 1) Hamiltonian matrix in real space, 2) Hamiltonian matrix in mode space. Smaller size of Hamiltonian matrices can increase the calculation speed since calculations are conducted on smaller matrices.

In this paper, the mode space form of Hamiltonian matrix is used on account of its 95% accuracy level and much less computation.
To illustrate this method, as shown in Fig. 2 the channel of transistor is considered as armchair GNR along with source and drain contacts.
This is a one-dimensional representation of a two-dimensional structure of GNR. Here the 2-D nanoribbon is considered as a quantum well along its width that forces the carriers to flow in some sub-bands. As mentioned earlier, with ballistic assumption, total Hamiltonian can be divided into independent matrices for each sub-band. As a result, the flow of the carriers in each sub-band may be calculated separately.

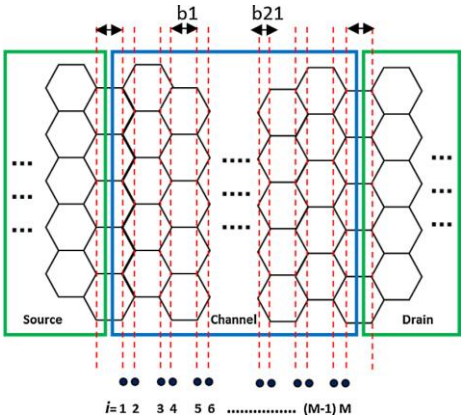

Fig. 2. Structure of an armchair Graphene nano-ribbon for calculating Hamiltonian in mode space.

The calculation of the Hamiltonian matrix for the first sub-band of the armchair Graphene nano-ribbon with n=12 is as follows [25]:

$$H=\begin{bmatrix} U_1 & b21 & & & & & \\ b_{21} & U_2 & b_1 & & & & \\ & b_1 & U_3 & b_{21} & & & \\ & & \ddots & \ddots & \ddots & & \\ & & & \ddots & \ddots & \ddots & \\ & & & & b_{21} & U_M & \end{bmatrix} \quad (2)$$

where U_i is the potential in the i-th loop, $b_{21}=2t\cos(4\pi/(n+1))$ is the coupling coefficient between two nearest neighboring loops, and $b_1=t(1+4C_{edge}\sin(4\pi/(n+1))^2/(n+1))$ is the coupling coefficient between two farthest neighboring loops in which t and C_{edge} are considered 2.7 eV and 0.12, respectively [26].

In order to calculate self-energy of the contacts, the following relations are used [27]:

$$\Sigma_{S(1,1)}=\frac{-A_S\pm\sqrt{A_S^2-4(E-U_1)^2b_1^2}}{2(E-U_1)} \quad (3)$$

$$\Sigma_{D(N,N)}=\frac{-A_D\pm\sqrt{A_D^2-4(E-U_N)^2b_1^2}}{2(E-U_N)} \quad (4)$$

$$A_{S(D)}=\left(\left(E-U_{1(N)}\right)^2-b_1^2-b_{21}^2\right) \quad (5)$$

The size of the self-energy matrices of the contacts equals the size of the Hamiltonian matrix of the channel. However, most of its elements are zero. For example, there is only one atom in the nanoribbon sheet coupled in the source side of the channel coupled to the contact. Therefore, only the (1,1) block in the self-energy matrix of the source contact is none zero. Similarly, in the self-energy matrix of the drain, only the (N,N) block is none zero [28].
In our calculations the Poisson equation is discretized by the finite difference scheme and solved self-consistently to obtain the potential within channel in an iterative procedure. After convergence, the Green's function problem is numerically calculated and after computing the aforementioned equations, the current flow from source to drain is measured by the following equation [23]:

$$I=\frac{2e}{h}\int_{-\infty}^{+\infty}T(E)\left(F(E-E_{FS})-F(E-E_{FD})\right)dE \quad (6)$$

where, e, h, F, E_{FS}, E_{FD}, and T(E) are electron charge, Planck's constant, Fermi distribution function, Fermi level of the source, Fermi level of the drain, and transmission coefficient, respectively.

3. **INTERACTION OF CARRIERS**

In order to include the effect of optical absorption in the channel, an additional term is introduced to the Green's function. We model this phenomenon as a scattering parameter which leads to generation of careers and consider it as a self-energy matrix along the channel. $\sum_{interaction}$ represents the self-energy function of the interaction of carriers and is included in relations as following:

$$G(E)=\left[\left(E+i0^+\right)-H-\sum_S-\sum_D-\sum_{interaction}\right]^{-1} \quad (7)$$

$\sum_{interaction}$ can be calculated from [23]:

$$\sum_{interaction}=-\frac{i}{2}\Gamma_{interaction} \quad (8)$$

$$\Gamma_{interaction}=\Sigma^{in}_{interaction}+\Sigma^{out}_{interaction} \quad (9)$$

$$\Sigma^{in}_{interaction}(E)=G^n(E-\hbar w) \quad (10)$$

$$\Sigma^{out}_{interaction}(E)=D^{ab}G^p(E+\hbar w) \quad (11)$$

D^{ab} is the absorption constant and $G^{n(p)}$ is the correlation function of electrons (holes) where $\Gamma_{interaction}$ is the broadening function due to electron-photon coupling. Eq.9 can be rewritten as [23]:

$$\Gamma_{interaction}(E)=D^{ab}[G^{n}(E-\hbar w)+G^{p}(E+\hbar w)] \quad (12)$$

In order to calculate G^n and $G^p$the following relations are used [23]:

$$G^{n}=G\sum^{in}G^{'} \quad (13)$$

$$G^{p}=G\sum^{out}G^{'} \quad (14)$$

$$\sum^{in}=\Gamma_S\times f_S+\Gamma_D\times f_D \quad (15)$$

$$\sum^{out}=\Gamma_S\times(1-f_S)+\Gamma_D\times(1-f_D) \quad (16)$$

$$f_S(E)=\left[1+\exp\left(\frac{E-\mu_1}{KT}\right)\right]^{-1} \quad (17)$$

$$f_D(E)=\left[1+\exp\left(\frac{E-\mu_2}{KT}\right)\right]^{-1} \quad (18)$$

$$\Gamma_S=i\times\left(\Sigma_S+\Sigma_S^{'}\right) \quad (19)$$

$$\Gamma_D=i\times\left(\Sigma_D+\Sigma_D^{'}\right) \quad (20)$$

In equations 17 and 18, f_S and f_D represent the Fermi functions, and the Fermi levels are denoted by $\mu_1$andμ_2.

$D^{ab}$is absorption constant which can be calculated from [23, 24]:

$$D^{ab}=N_w D_0(\hbar w) \quad (21)$$

$$N_w=\left[\exp\left(\frac{\hbar w}{K_B T}\right)-1\right]^{-1} \quad (22)$$

$$D_0=\frac{\hbar j_1^2|M|^2}{2nm_c w} \quad (23)$$

where j_1=6 ev/Å is hoping parameter, |M| is the optical transition matrix element, N_w is the equilibrium Bose-Einstein distribution of photons and m_c is the mass of carbon atom, respectively [25, 26].

$\sum_{interaction}$is calculated employing equations 8-23 in an iterative progress. G(E) can be obtained from equation 7 using $\sum_{interaction}$, and it can be employed to calculate the current flow from equation 6.

By calculation of the photo-current of the device, its performance can be analyzed.

4. **RESULTS AND DISCUSSIONS**

We do the simulations for the proposed photo-transistor with GNR channel of n=12 and a ribbon bandgap of 0.6 eV. The oxide surrounding the channel is

chosen as Hafnium oxide with a dielectric constant of 16 and a thickness of 2 nanometers.

By calculation of the current without the effect of optical absorption ($\sum_{interaction}=0$), the dark current of the detector is obtained. Fig. 3 shows dark current characteristic as a function of drain voltage and for different gate voltages. As can be seen the current increases with drain voltage and saturates at higher voltages because of limited number of carriers. The figure also shows that for higher gate voltages the current is increased. This is due to the fact that for increased gate voltages, more carriers accumulate under the gate and incorporate in current generation. In order to obtain the responsivity which is a main characteristic of a detector, its photocurrent should be calculated. To do so, in this section, we include the effect of optical absorption along the channel in the calculations. Photocurrent of the detector vs. the drain voltage is depicted in Fig. 4 for different incident optical powers where the gate voltage is held on V_{gs}=0.4V .P_{op}=0 results in the dark current.

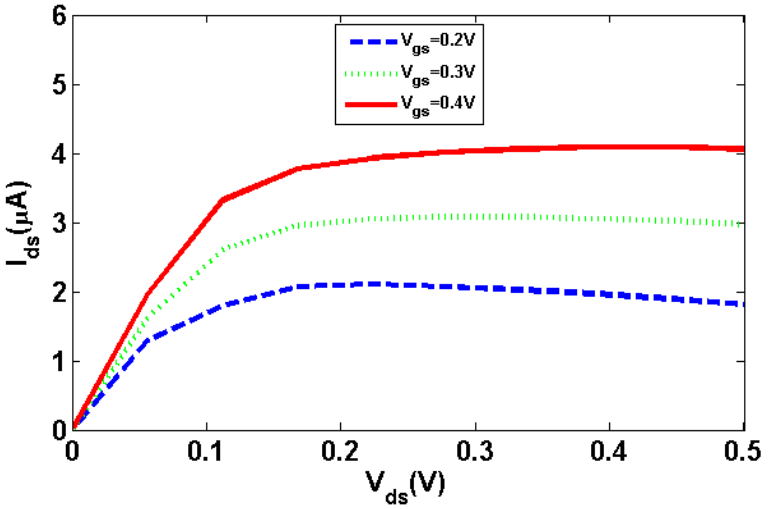

Fig. 3.Dark current vs. drain voltage for different gate voltages.

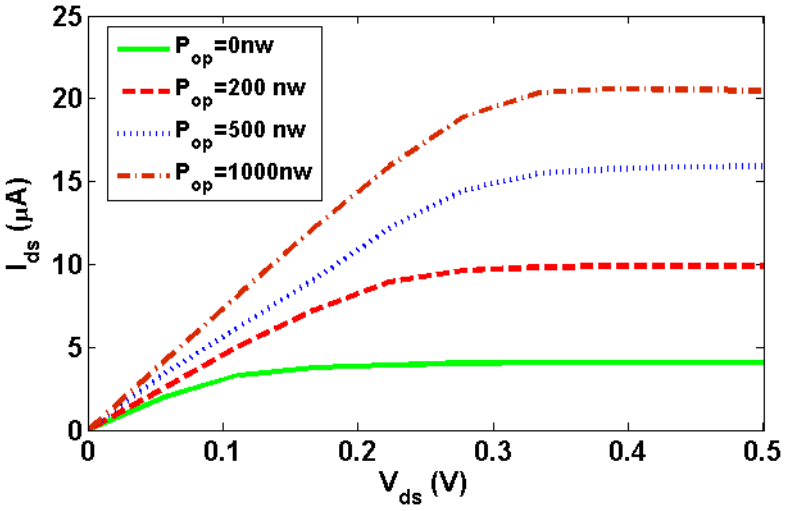

Fig. 4. Photocurrent with respect to drain voltage at on and for different optical input powers.

The figure reveals that a considerable change in current occurs when the photo-transistor is exposed by an optical power. As the optical input power increases, the photocurrent gets higher orders because of contribution of photo-generated carriers in current flow. However the photo-current saturates at higher voltages similar to the dark current. This can be due to the excitation of all electrons in valance band and their contribution in photo-current. Although we didn't find any similar structure with experimental results to compare to our model, however the order of obtained dark and photocurrents obtained from the proposed model are in agreement and proximity to some previous studies [32].

We tried the calculations for different gate voltages and the results are in Fig. 5. From the figure at a fixed incident optical power any increase in gate voltage leads to formation of higher current. This figure reveals that both the optical power and gate voltage increase the photo-current.

Fig. 6 presents dependence of the photo-current on input power and studies it for different drain voltages. As expected the photo-current increases with optical power but the slope of changes is larger for higher drain voltages. The results shown in this figure are in close agreement to the experimental studies [33].

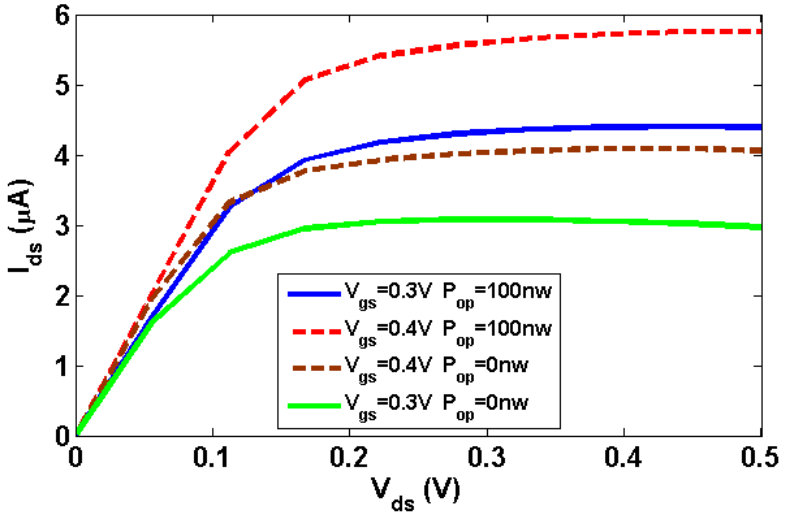

Fig. 5. Photocurrent for different gate voltages and optical input powers.

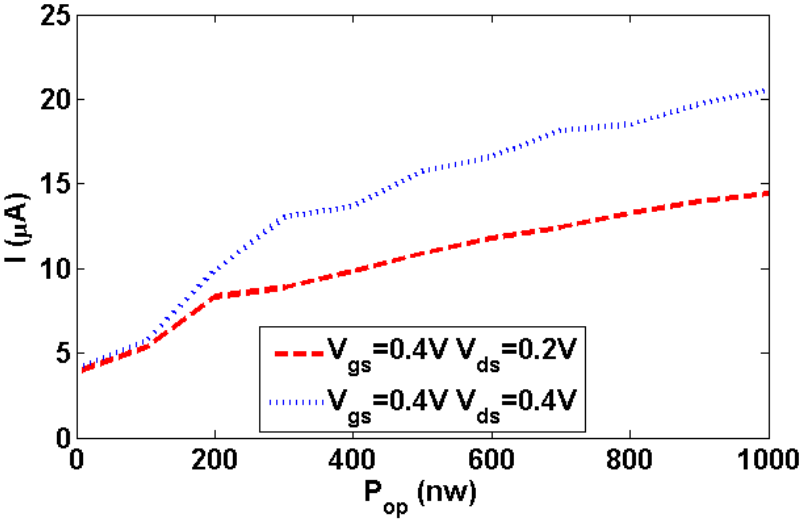

Fig. 6.Photo-current as a function of input optical power and for different drain voltages.

CONCLUSIONS

A theoretical study of GNR based photo-transistors was performed by numerical modeling of their performance characteristics. In the presented model non-

equilibrium Green's function method was used to study the carrier transport in the structure of device and the optical performance of the detector is modeled by inclusion of a self-energy matrix in the relations as the electron-photon interaction matrix along the channel. Results show that higher photo-current flows when the device is exposed by an optical input. However the photo-current saturates at higher voltages similar to the dark current.

REFERENCES:

[1]. H. Lu, "Plasmonic characteristics in nanoscale graphene resonator-coupled waveguides," Appl. Phys. B **118**, 61-67 (2015).
[2]. F. Ostovari and M. K. Moravvej-Farshi, "Dual function armchair graphene nanoribbon-based spin-photodetector: optical spin-valve and light helicity detector," Appl. Phys. Lett **105**, 072407-072401 (2014).
[3]. C. H. Liu, Y. C. Chang, T. B. Norris, and Z. Zhong, "Graphene photodetectors with ultra-broadband and high responsivity at room temperature," Nature Nanotech. **9**, 273–278 (2014).
[4]. A. Y. Goharrizi, M. Pourfath, M. Fathipour, and H. Kosina, "Device Performance of Graphene Nanoribbon Field-Effect Transistors in the Presence of Line-Edge Roughness," IEEE Trans. Electron. Dev. **59**, 3527 - 3532 (2012).
[5]. R. F. M. Rostami, H. Rabiee Golgir, "Magnetization of bilayer graphene with interplay between monovacancy in each layer," J. Appl. Phys. **114**, 084313-084311-084313-084315 (2013).
[6]. C. Berger, Z. Song, X. Li, W. Wu, N. Brown, C. Naud, D. Mayou, T. Li, J. Hass, A. N. Marchenkov, E. H. Conrad, P. N. First, and W. A. d. Heer, "Electronic Confinement and Coherence in Patterned Epitaxial Graphene " Science 312 1191-1196 (2006).
[7]. P. Avouris, Z. Chen, and V. Perebeinos, "Carbon-based electronics," Nature Nanotech. 2, 605 - 615 (2007).
[8]. J. Shang, T. Yu, and G. G. Gurzadyan, "Femtosecond energy relaxation in suspended graphene: phonon-assisted spreading of quasiparticle distribution," Appl. Phys. B **107**, 131-136 (2012).
[9]. K. Nakada, M. Fujita, G. Dresselhaus, and M. S. Dresselhaus, "Edge state in graphene ribbons: Nanometer size effect and edge shape dependence," Phys. Rev. B 54, 17954 (1996).
[10]. H. Mohamadpour and A. Asgari, "Graphene nanoribbon tunneling field effect transistors," Physica E **46**, 270–273 (2012).

[11].J. Capmany, D. Domenech, and P. Muñoz, "Silicon graphene waveguide tunable broadband microwave photonics phase shifter," Opt. Express **22**, 8094-8100 (2014).
[12].P. B. Bennett, Z. Pedramrazi, A. Madani, Y.-C. Chen, D. G. d. Oteyza, C. Chen, F. R. Fischer, M. F. Crommie, and J. Bokor, "Bottom-up graphene nanoribbon field-effect transistors," Appl. Phys. lett. **103**, 253114-253111-253114-253114 (2013).
[13].F. Bonaccorso, Z. Sun, T. Hasan, and A. C. Ferrari, "Graphene photonics and optoelectronics," Nature Photon. **4**, 611 - 622 (2010).
[14].R. F. H. Rabiee Golgir, M. Pazoki, H. Karamitaheri, R. Sarvari, "Investigation of quantum conductance in semiconductor single-wall carbon nanotubes: Effect of strain and impurity," J. Appl. Phys. **110**, 064320-064321-064320-064326 (2011).
[15].A. R. Wright, J. C. Cao, and C. Zhang, "Enhanced optical conductivity of bilayer graphene nanoribbons in the terahertz regime.," Phys. Rev. Lett. 103, 207401 (2009).
[16].J. M. Dawlaty, S. Shivaraman, J. Strait, P. George, M. Chandrashekhar, F. Rana, M. G. Spencer, D. Veksler, and Y. Q. Chen, "Measurement of the optical absorption spectra of epitaxial graphene from terahertz to visible," Appl. Phys. Lett 93, 131905 (2008).
[17].J. Li, L. Niu, Z. Zheng, and F. Yan, "Photosensitive Graphene Transistors," Adv. Mater. **26**, 5239–5273 (2014).
[18].X. Gan, R. J. Shiue, Y. Gao, I. Meric, T. F. Heinz, K. Shepard, J. Hone, S. Assefa, and D. Englund, "Chip-integrated ultrafast graphene photodetector with high responsivity," Nature Photon. **7**, 883–887 (2013).
[19].F. Withers, T. H. Bointon, M. F. Craciun, and S. Russo, "All-Graphene Photodetectors," ACS Nano **7**, 5052–5057 (2013).
[20].A. U. M. Furchi, A. Pospischil, G. Lilley, K. Unterrainer, H. Detz, P. Klang, A. M. Andrews, W. Schrenk, G. Strasser, T. Mueller, "Microcavity-Integrated Graphene Photodetector," Nano Lett. **12**, 2773–2777 (2012).
[21].Q. Gao and J. Guo, "Quantum mechanical simulation of graphene photodetectors," J. Appl. Phys. **112**, 084316-084311-084316-084316 (2012).
[22].E. Ahmadi and A. Asgari, "Modeling of the infrared photodetector based on multi layer armchair graphene nanoribbons," J. Appl. Phys. **113**, 093106-093101-093106-093107 (2013).
[23].S. Datta, *Quantum Transport: Atom to Transistor* (Cambridge, 2005).
[24].M. Pourfath and S. Selberherr, "Current Transport in Carbon Nanotube Transistors," in *7th International Caribbean Conference on Devices, Circuits and Systems*, 2008),
[25].G. D. Mahan, "Electron–optical phonon interaction in carbon nanotubes," Phys. Rev. B **68**, 125409-125401-125409-125405 (2003).

[26].S. O. Koswatta, M. S. Lundstrom, and D. E. Nikonov, "Band-to-Band Tunneling in a Carbon Nanotube Metal-Oxide-Semiconductor Field-Effect Transistor Is Dominated by Phonon-Assisted Tunneling," Nano Lett. **7**, 1160–1164 (2007).